LAWRENCE
LIVERMORE
NATIONAL
LABORATORY

LLNL-JRNL-666426

Simulation Of The Main Physical Processes In Remote Laser Penetration With Large Laser Spot Size

S. A. Khairallah, A. Anderson, S. Rubenschik, J. Florando, S. Wu, H. Lowdermilk

January 22, 2015

American Institute of Physics Advances

Disclaimer

Simulation Of The Main Physical Processes In Remote Laser Penetration With Large Laser Spot Size

Saad A. Khairallah, Andrew Anderson, Sasha Rubenschik, Jeff Florando, Sheldon Wu, Howard Lowdermilk

Lawrence Livermore National Laboratory, 7000 East Ave. Livermore, CA 94550

Corresponding author: Saad A. Khairallah. Tel: 1-925-422-0675.

E-mail addresses: khairallah1@llnl.gov (Saad A. Khairallah), anderson1@lln.gov (Andy Anderson), rubenchik1@llnl.gov (Sasha Rubenchik), florando1@llnl.gov (Jeff Florando), wu31@llnl.gov (Sheldon Wu), lowdermilk1@llnl.gov (Howard Lowdermilk).

ABSTRACT

A 3D model is developed to simulate remote laser penetration of a 1mm Aluminum metal sheet with large laser spot size (~ 3x3cm^2), using the ALE3D multi-physics code. The model deals with the laser-induced melting of the plate and the mechanical interaction between the solid and the melted part through plate elastic-plastic response. The effect of plate oscillations and other forces on plate rupture, the droplet formation mechanism and the influence of gravity and high laser power in further breaking the single melt droplet into many more fragments are analyzed. In the limit of low laser power, the numerical results match the available experiments. The numerical approach couples mechanical and thermal diffusion to hydrodynamics melt flow and accounts for temperature dependent material properties, surface tension, gravity and vapor recoil pressure.

Keywords: Fluid dynamics, Laser, Remote Laser penetration and melting, Heat transfer, First-principles simulation

0. INTRODUCTION

Advances in high power fiber lasers and solid-state lasers with improved beam quality and elongated focal lengths are enabling new remote laser processing capabilities. Macken (Macken, 1996) was among the first to report on these advances and their application to the automobile industry not long ago in the late 1990. Zaeh et al (M. F. Zaeh, 2010) enumerated the current cutting edge technology in remote laser processing namely welding and two cutting processes. He asserts that remote welding alone may be considered an evolution of the conventional laser welding or, a revolution, if taken together with the advanced research that impacted the optical laser system peripherals (high speed and acceleration digital scanners, galvanometers, dynamic deflection). On the other hand, the two new remote cutting processes: remote ablation cutting (RAC) and remote fusion cutting (RFC), differ significantly from conventional laser cutting.

Conventional welding and cutting processes are actually close to each other. The difference being, with conventional cutting, the molten material must be immediately blown out by a gas jet to create a clean narrow kerf. Otherwise, the result would be a deep fusion penetration just like in a weld. A remote process implies that longer working distances (distances easily greater than one meter and in fact, can reach several kilometers depending on the application) make it unpractical, if not impossible, to use

pressurized process gas supplied through the optical system. Hence, different physical processes have to replace the effect of the gas jet to enable remote cutting.

With the RAC process, as described by Steen in (Steen, 2003), the laser power is on the order of few kW, concentrated over a spot of diameter 50-100μm. The resulting intensity of $10^8 W/cm^2$ is enough to evaporate the material over a narrow region. Some of the evaporated material builds up a gas pressure, at the bottom of the cut that pushes the melt further up along the walls of the kerf and help deepen the cut. The depth increases by reiterating with several high scan speed (360-720m/min) laser passes. Klotzbach et al (A. Klotzbach, 2009) and Wagner et al (A. Wagner, 2013) showed good results from a process that employs a high cutting speed, which yields minimal heat affected zone (HAZ), and a cheap fast turnout of a high quality cut.

Matti et al (R. S. Matti, 2013) describes the RFC process as more complex. The sheet thickness determines the process parameters. The spot diameter is around 600μm and the laser intensities achieved are a bit lower $10^6 W/cm^2$. However the scan speed of 4-12 m/min is much lower than in RAC. Hence, more energy is deposited into the material resulting in a large HAZ and a keyhole -like regime. Eventually, a continuous gas cavity forms, linking the top to the bottom side of the sheet. While some material is ejected from the top, other melt on the bottom gets flushed down with the help of vapor recoil pressure and gravity. For Matti et al (R. S. Matti, 2013), this physical ejection mechanism is still not completely understood and further modeling is required for deeper and more accurate analysis.

These remote processes are starting to be the subject of research and scrutiny (A. Wagner 2013, R. S. Matti 2013) while being implemented in industrial production (A. Klotzbach 2009) by trial and error. The current study deals with a problem close to RFC. The only difference is the laser spot size used in this article is a lot larger, on the order of few cm^2. This is driven by applications that aim at clearing well mouths from damaged equipment during emergency and recovery work in oil and gas fields and dismantling radioactive structures found in obsolete nuclear plants first described by Tahmouch et al (G. Tahmouch, 1997) and Antonova et al (G. F. Antonova, 1999) or at demining from a safe distance by using extremely powerful solid-state laser developed by a team of Livermore physicists and engineers as reported by Heller in a series of Lawrence Livermore National Laboratory Science and Technology Review articles (Heller, Laser Burrows into the Earth to Destroy Land Mines 2004, Heller, Transparent Ceramics Spark Laser Advances 2006). This effort won a 2004 Research and Development 100 Award for its promise of revolutionizing the practice of demining.

As a first effort in this direction, a series of experiments is devised to study the effect of laser interaction with a thin sheet of Aluminum, 1mm thick (See **Figure 1**). The laser intensity used is in the low range ($200 W/cm^2$); however, by compensating with a long laser dwell time, the laser manages to penetrate the plate. This is accompanied by the formation of a main molten blob with few fragments that swing and drop in random directions. A thin layer of metal-oxide remains over the irradiated area after the underlying aluminum has melted. The experimental setup for **Figure 1** and main results that discuss the effect of the oxide layer on laser's ability to penetrate the plate will be detailed in a separate publication.

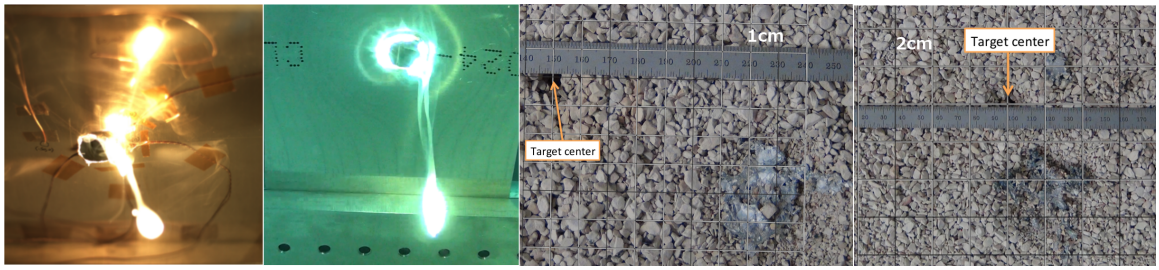

Figure 1. Penetration experiments where 1-mm thick aluminum samples are illuminated by 0.8μm laser light at intensities up to 200W/cm^2, levels that are much lower than found in RAC or RFC, but the time to melt separation is 10 seconds and full (A.M. Rubenchik 2014)exposure is close to a minute. The two-left most figures illustrate the formation of a main fragment/droplet of material and falling in a swinging motion at an offset from the target center. The two right-most figures show the main large droplet landing at an offset from the target center. The right most figure shows an extra landing site for a second small droplet fragment.

Most theories that try to explain the dynamical laser material interactions introduce simplifying assumptions, whether it being decreasing the dimension of the problem from 3D to 2D or 1D or neglecting some other physics such as melt flow or thermo-mechanical coupling, in order to come up with a manageable and solvable set of equations. Igor Smurov goes into the details of many of these theories in his book, (Smurov, 2011). The approach in this study is to simulate the remote laser penetration/cutting process with large laser spot and capture the main physical processes leading to rupture with a minimal set of approximations.

1. LASER-PLATE INTERACTION MODEL SETUP

A simulation model of laser-matter interaction for a moderate CW laser flux (300 – 2000 W/cm^2) is developed. The physical process is complex and depends on temperature, laser power, and material properties. The surface tension plays an important role in the melt dynamics coupled to a thermo-mechanical response of the material. To learn about these effects separately, a graded approach is adopted, which exposes the role of the various physical processes by refining the physics modeling one step at a time. Hence, three main successive models are presented. At first, the melt dynamics in the absence of surface tension is studied. Second, a temperature dependent surface tension is added to the model. Third, the vapor recoil pressure is accounted for. At each step, different combinations of laser power and laser spot size are considered, both with and without the effects of gravity.

The simulations are performed in an arbitrary Lagrangian-Eulerian (ALE) mode, using ALE3D (McCallen, 2012), which is a multi-physic numerical simulation code developed at Lawrence Livermore National Laboratory. ALE3D follows a rigorous verification and validation effort and was recently used to simulate Selective Laser Melting of Stainless Steel powder with good agreement with experimental results (Khairallah, 2014).

The primary limitation of the explicit hydrodynamics in this application is the limit on the time step size imposed by numerical stability constraints. The well-known Courant-Friedrichs-Lewy (CFL) condition limits the time step size to be less than the transit time of a sound wave across the smallest element. The spatial discretization is determined by the number of elements chosen for the thickness of the plate. Three zones across the

experiment's 1mm thick plates were enough to resolve the main features of the melting process. In addition to this, since the main melt dynamics take place at the center of the cylinder, finer zoning towards the center is applied compared to the remainder of the plate. This problem setup requires a time step close to 6ns and results in a problem size of up to half a million elements, factors which lead to lengthy simulation run times. To speed up the simulations, the problem is domain decomposed and processed in parallel by 48 processors. Also, to obtain larger time step sizes, a variant of density scaling as described by Khairallah and Anderson in (Khairallah, 2014) is used; a reasonable time scaling limit was found in the range of five to ten. Higher values introduce more speedup but cause noticeable changes in the melt dynamics.

Temperature [K]	**300**	**400**	**500**	**600**	**700**
Density [g/cc]	2.7	2.67	2.656	2.631	2.614
Heat Capacity at constant pressure [J/kg K]	896.5	963.5	989.7	1000.0	1132.0
Thermal Conductivity [W/m K]	123.0	141.0	174.0	183.5	174.0

Table 1. Material properties. The density and heat capacity are extracted from the Sesame equation of state table which is maintained by Los Alamos National Laboratory. The surface tension is taken from (Enrica Ricci, 2013) **and the viscosity from** (A.T. Dinsdale, 2004)**.**

The simulation model consists of an aluminum (see **Table 1**) plate defined on a quarter-cylindrical mesh and surrounded above and below by void (see Figure 2). The plate

edges are rigidly constrained. Symmetry boundary conditions are applied to the faces of the quarter cylinder. The laser source consists of simple parallel rays that heat the surface of the material within a uniform spot size. Different spot sizes are considered, 4x4cm^2 as in the experimental setup, as well as 3x3cm^2 and 2x2cm^2. The results mostly reported are for the 3x3cm^2 case unless stated differently.

The laser absorptivity is one of the main uncertainties in simulations of laser material interactions. It is hard to measure experimentally since it depends on several factors(A.M. Rubenchik). It was reported previously (Khairallah, 2014) that an average material absorptivity works fine. Hence, a constant absorptivity of 0.33 is adopted.

Different laser powers are considered starting from a minimum of 4.4kW, which gives about 490 W/cm^2 at the 3x3cm^2 spot size. This is above the 200 W/cm^2 used for the experiment described in **Figure 1**. The low intensity laser simulation results are extrapolated to the experimental observations in **Figure 1** and similar characteristic fragment formation is noted. This choice is dictated by the cost of matching simulation time scale (see discussion above) to the experimental one, which runs close to a minute. Higher power accelerates the process of melting and therefore decreases the runtime close to 20,000-40,000CPU hours.

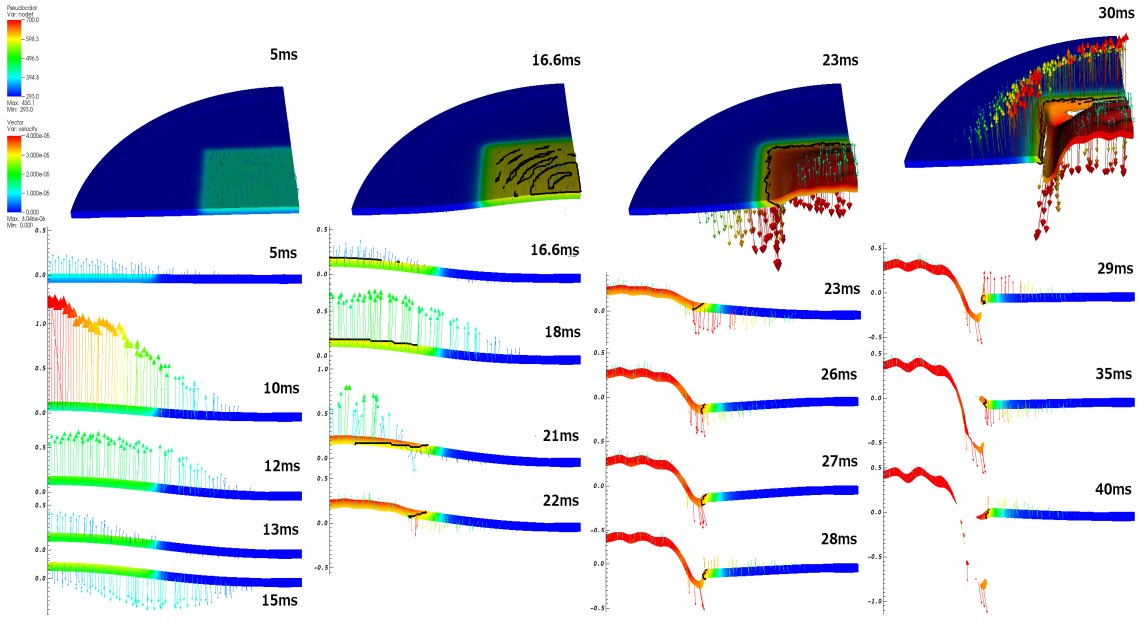

Figure 2. Zero surface tension model with gravity. A series of snapshots of a $4.4kW$ laser with a $3x3cm^2$ spot size impinging on a $1mm$ Al plate. They show the buckling along with plate oscillations and eventual melting and detachment of the melt. Since the velocity ($cm/\mu s$) increases a lot after 22ms, the velocity vectors are scaled down by a factor of 10 in 2D and 2.5 in 3D. NodeT indicates nodal temperature (in Kelvin). The black contour line indicates 0 shear modulus, that is melting (~ $700K$). These scale settings are applied to all figures in this paper.

2. NO SURFACE TENSION

The effect of neglecting surface tension in the laser-plate interaction is first studied in Figure 2. Four stages can be distinguished. In the first 15ms, the plate reacts to the deposited laser energy by buckling upward and oscillating around z~2mm. Since it is constrained in the x and y directions, the expansion has to occur in the z direction. Given that the heat is deposited at the top of the plate, the bottom stays colder and a net expansion favors the +z direction. The sudden upward response is brought to rest by the

restoring elastic stresses in the plate. The ensuing motion is a damped oscillation around the maximum deflection point close to 2mm. Plotting the total kinetic energy (KE) in Figure 3 is another way to observe this behavior. The KE starts from 0 for the plate at rest, and then increases due to acquired momentum from the expansion. Soon after, a damped oscillation sets in until 16.6ms.

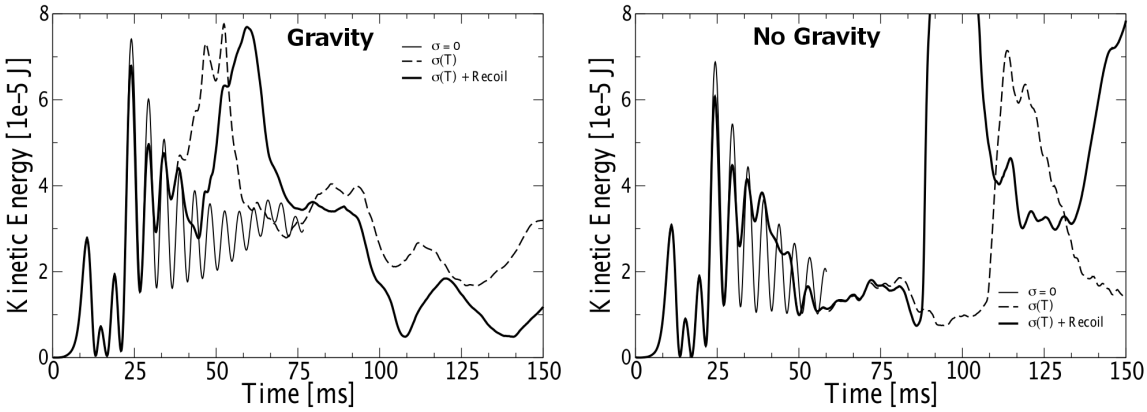

Figure 3. Dependence on Gravitation of the three main models: zero surface tension (σ=0), temperature dependent surface tension (σ(T)) with and without vapor recoil pressure. The curves overlap up to 30*ms* when (σ=0) curve separates from the rest. Gravity becomes important at long time scales and helps induce plate rupture, sooner than in the case of no Gravity. The sudden increase in kinetic energy observed after the onset of oscillations is a sign of plate rupture, which is immediately accompanied by sudden high melt acceleration along the ruptured surface due to surface tension. Of course, this signature is absent in the zero surface tension models.

Around 16ms, the first signs of melting on the top plate surface are shown as black contour lines in Figure 2. The plate is softening under the heat, which decreases its stiffness and releases more thermal stresses. These contribute to the amplitude of the restoring oscillations. Eventually, close to 21ms, the plate's center bottom starts melting too and the melt region reaches quickly, within 1ms, the rim of the laser spot. This suddenly frees more stresses from the buckled region and initiates stronger oscillations.

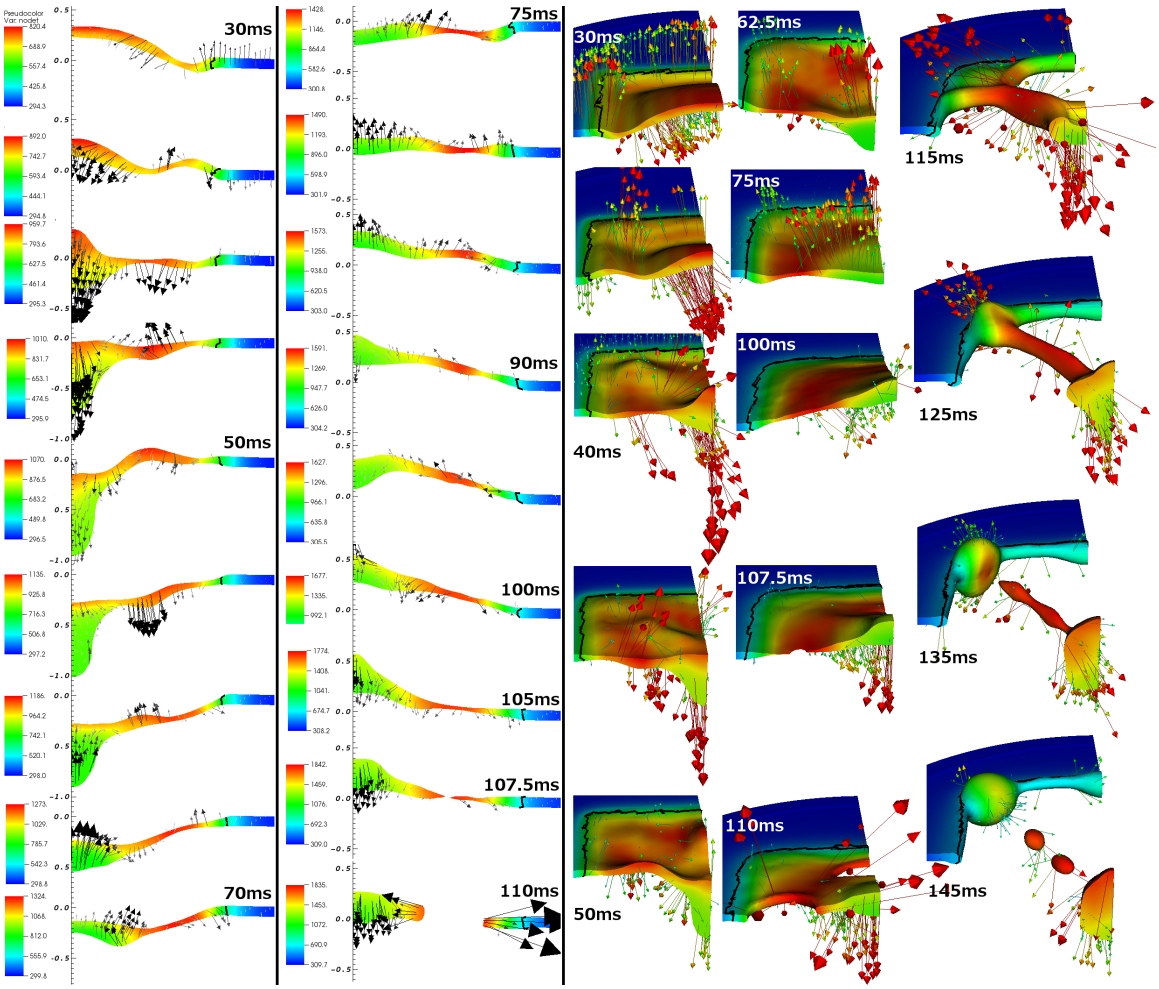

Figure 4. Laser-plate interaction model with temperature dependent surface tension in the absence of gravitation. The velocity color-coding follows the same scale as in Figure 2, **except that a black color is picked for the 2D vector projection pictures for better visibility. The snapshots are taken at 5ms consecutive time intervals unless noted otherwise. The black contour line separates solid material from melt. The 2D/3D snapshots show the transfer of plate oscillations to the melt, evolution of the melt oscillations, thinning and initiation of breakup into droplets. The plate rupture occurs in a hot band between the center and the laser spot edge. The Marangoni effect draws more material flow to the cooler part along the perimeter of the laser spot and to the bottom of the material at the center. The Plateau-Rayleigh instability is responsible of breaking the cylinder melt along the diagonal (at 125*ms*-145*ms*) into a large droplet and smaller fragments. In the presence of gravity (not shown here), the melt flows towards a sinking center, which leaves less material to create small fragments.**

This is also marked by a slight increase in KE as Figure 3 indicates. These oscillations remain damped though, since the solid square edges are still in touch with some melt. Note that the effect of the gravitational force at this stage is minimal as the small differences between the zero surface tension curves in Figure 3 indicate. This is because the time scales are short, on the order of 1ms. In contrast, it takes gravity over 200 ms to move an object by 2.5 mm from rest.

After 23ms, the newly developed strong oscillations seen at the solid edges of the plate start getting decoupled from the melt, which of course holds no strength, and therefore can not keep up with the oscillatory motion. Figure 2 shows how this decoupling takes place. Between 23ms and 29ms, the rim performs one complete oscillation, while the melt in touch with the solid rim is moving down with the momentum it acquired at 23ms. The tearing is initiated around 29ms, during the upward swing of the plate, and proceeds to the 90^{o} degree corner of the square spot, where there is more material and therefore more time is needed for thinning.

3. TEMPERATURE DEPENDENT SURFACE TENSION

Next, the physics modeling is refined by including temperature dependent surface tension (see **Figure 4**). This model evolves differently from the previous model (**Figure 2**). While the plate oscillations still play an important role, the decoupling from the melt is harder since the oscillations have to circumvent an additional force, that of the surface tension of the melt. This force keeps the melt attached to the plate; hence it transfers the plate oscillations to the melt and dampens the oscillation amplitude. This force delays the

breakup until late in time, at 110*ms* as opposed to 30*ms* for the previous model (**Figure 2**). The damping is a consequence of nature's energy minimum principal. The surface energy of a plane is lower than one with ripples. Hence, the surface tension acts to suppress high amplitude oscillations down to the plane. This damping can clearly be observed by looking at the amplitude difference in KE between σ(T) and σ=0 curves after 30*ms* in **Figure 3**.

Another effect that is at play is hydrodynamics flow due to high temperature gradients (on the order of ~ 100*K*/*mm* and more). Since surface tension decreases with increasing temperatures, cold regions have higher surface tension than hot ones. This creates surface tension gradients that move material from hot to cold regions on the surface and reshapes the melt (Marangoni effect). This effect would have been more pronounced had a Gaussian laser been used. However, the spot illuminated by the uniform laser still exhibits temperature gradients as **Figure 4** shows. The snapshots leading to the breakup at 107.5*ms* show that the hottest zone is not the center of the square spot, but rather in the band of thinning material between the solid plate edges and the center. The velocity vector fields show surface flow in addition to the effects of the oscillations. Although less pronounced in magnitude compared to the vertical oscillatory motion, the material flows away from the band, towards the center and the plate edge. Since the bottom of the plate is not directly illuminated, it tends to be cooler than the surface, for a reasonable thickness of more than 3μm. This causes the cooler bottom center region to swell as it attracts material from the thinning hot band region. The thinning of the band eventually leads to an effective local low thermal conductivity, which acts as a bottle neck for the heat dissipation, and of course accumulates further heat at the band, and in turn will

decrease the surface tension and cause further thinning. This leads to surface tearing as observed at 107.5*ms* in Figure 4.

As soon as the surface is torn, the surface tension accelerates the melt along the torn surface towards the plate diagonal and forms a cylindrically shaped body of fluid. Since the surface energy of a sphere is lower than that of a cylinder, this portion of the melt breaks further into droplets. This phenomenon is reminiscent of the Plateau-Rayleigh instability. Plateau and Rayleigh showed that a perturbation mode, with a wavelength around three times the radius of a liquid cylinder, would dominate all other perturbation modes and eventually break a liquid cylinder into droplets, as depicted in Figure 4. Note that, the melt break up and the subsequent motion are symmetric and this is particular to the current model. In reality, surface and laser anisotropies will act to break this symmetry. Other simulations are performed (not shown) with uneven laser heating. They show irregular melt flow that pushes material towards the solid plate edge, where large droplets form and precipitate downward when driven by gravity or recoil pressure.

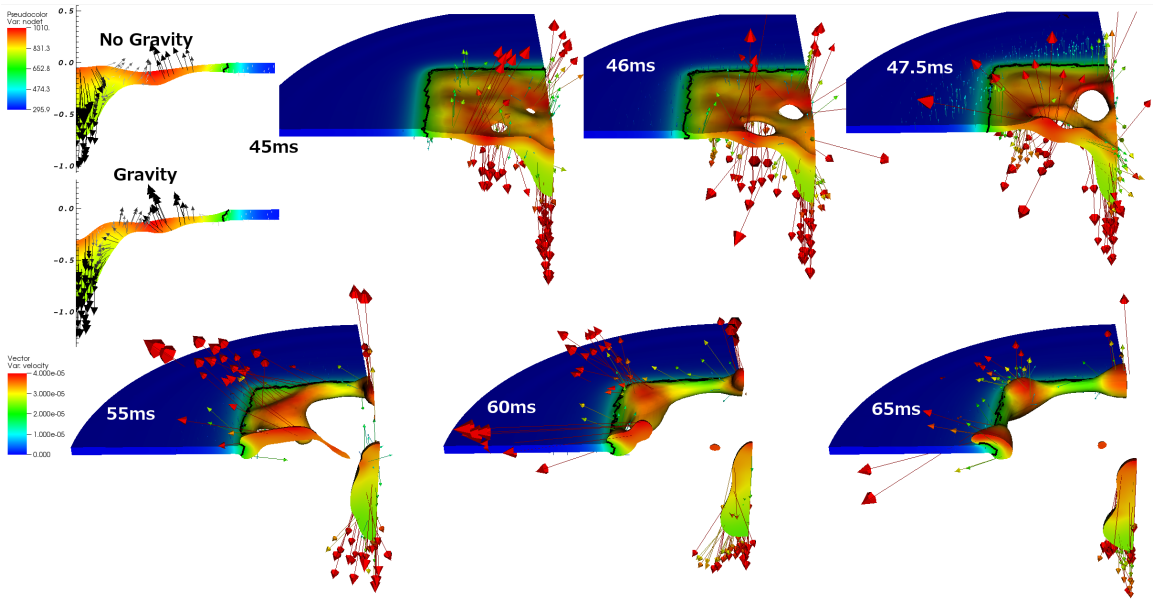

Figure 5. Laser-plate interaction model with temperature dependent surface tension and recoil pressure in the presence of gravitation. The top left 2D slice figures show the difference when gravity is ignored at 45ms. Compared to Figure 4, gravity and vapor recoil pressure cause an earlier surface rupture. Also, the gravitational force initiates a material flow to the sinking center and causes the satellite fragments to shrink in size since less material is left for their formation. The recoil pressure acts in unison with gravity in accelerating the fragments down.

4. TEMPERATURE DEPENDENT SURFACE TENSION WITH GRAVITY AND VAPOR RECOIL PRESSURE

The next refinement in the model includes the effect of gravity and vapor recoil pressure (see **Figure 5**). The latter is due to material evaporating and imparting a recoil momentum, which generates a recoil pressure P given by

$$P = 0.54 P_a e^{-\frac{\lambda}{K_B}\left(\frac{1}{T}-\frac{1}{T_b}\right)},$$

where P_a=1e-6*Mbar* is the ambient pressure, λ=3.225*ev/atom* is the evaporation energy per Aluminum atom, K_B=8.617e-5*ev/K* is Boltzmann constant, T is the surface temperature and T_b=2740*K* is the boiling temperature of Aluminum. The effect of recoil is expected to complement that of the gravitational force, since they both act in the same direction. When very high surface temperatures close to boiling are achieved, the recoil force becomes larger than the surface tension, which decreases linearly with temperature. The recoil force is then more efficient at rupturing the thin hot band at the edge of the melted region. The laser power is not high enough in the Figure 5 simulation to achieve high surface temperatures and therefore gravity is the dominant force after surface tension. For lower laser power, the surface melt holds long enough for gravity to start acting on the flow. In Figure 5 2D slice simulations at 45ms, gravity pulls the flow downward by few millimeters. This, combined with the thinning of the hot band discussed above contributes to an even earlier rupture occurring at 45ms. This is because gravity stretches the melt surface down, hence further thinning the material in the band region. Without gravity, the melt surface is less stretched and remains closer to the initial horizontal

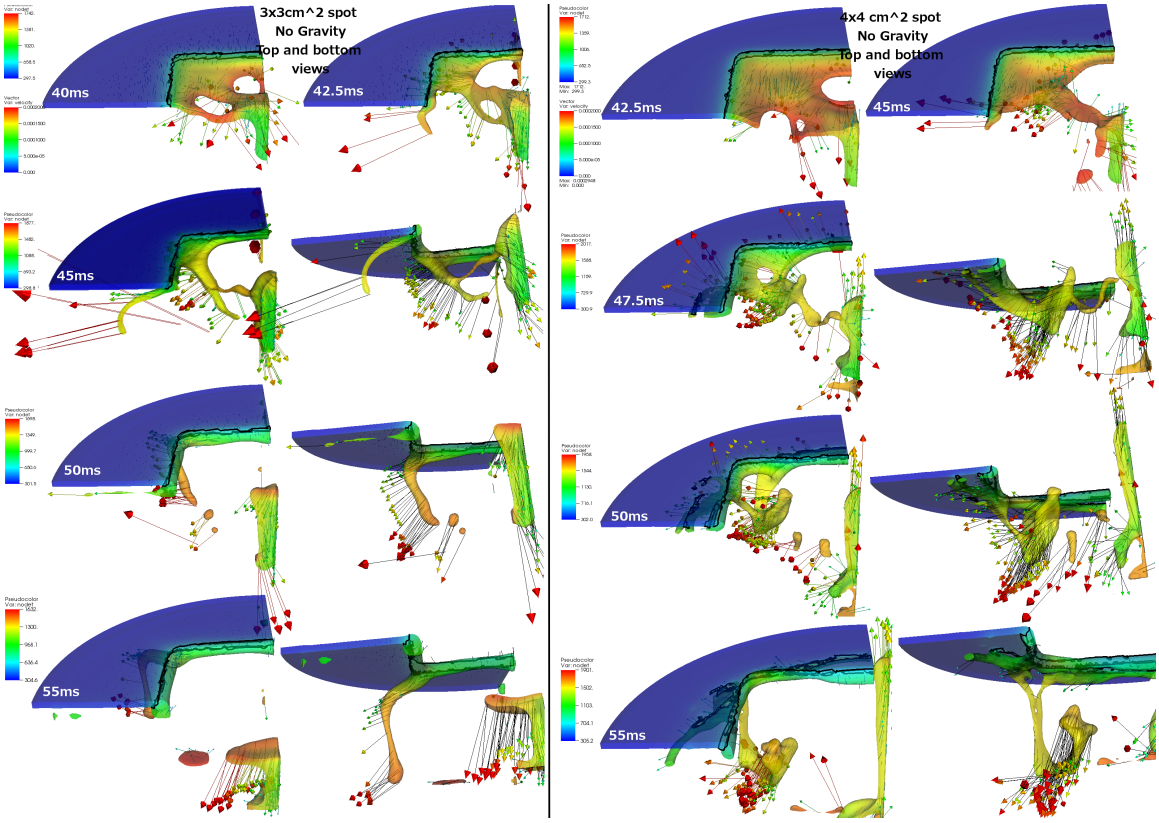

Figure 6. Laser-plate interaction in the case of high laser power and increasing spot size. The simulations are performed in the absence of gravity for a 3x3cm^2 laser spot size at a laser power of 9.9kW and 4x4cm^2 laser spot size at a laser power of 17.6kW. The snapshots are arranged in columns. Each row starts with a top view snapshot followed on the right, when useful, with bottom view snapshot at the same time. The figures are semi-transparent to enable better visualization of the melt swinging towards the cold side of the plate. Some debris is seen landing on the bottom side of the box. The large spot size melts more material, which creates bigger and more fragments. Also, the high intensity simulations show two main droplets forming, one at the center that is accelerated downward and another one that swings along the diagonal toward the cold plate.

plane, hence the rupture occurs 40ms later in time as the kinetic energy jump indicates close to 85ms in Figure 3. Note that the results without gravity in Figure 3 show 25ms early rupture with recoil. This is because the recoil pressure acts in the same direction as gravity. In the presence of gravity, the rupture with recoil happens 15ms later than the

case without recoil. This is a bit unintuitive. However, this is due to the fact that the recoil force is non-uniform due to a non-uniform surface temperature. Combined with the oscillations, the rupture becomes a random event.

Another difference observed in the gravitational model in **Figure 5** is the melt dynamics after rupture. Some surface melt retreats to the cold plate edges. Also a larger droplet forms in the center. In fact, this droplet is the final evolution of a melt dripping that formed due to increased material flow to the center initiated by the gravitational downward pull and Marangoni effect (see discussion above). The melt dynamics resembles the experimental observations (**Figure 1**).

5. DEPENDENCE ON PLATE SIZE AND LASER POWER

The effect of recoil pressure is explored in Figure 6 by performing simulations at higher laser power (9.9kW and 17.6kW). The experimental observation of melts swinging upon rupture and other random debris jettisoned randomly is more evident in the simulations for Figure 6. Since gravity and recoil pressure have the same downward push, gravity is excluded just to isolate the pure recoil pressure effect. The surface melts fast and the first signs of surface rupture occur quite early at 40ms for a laser spot size of $3x3cm^2$ and 2.5ms later for the larger size of $4x4cm^2$. Including gravity does not change the following observations since it is negligible for this short time scale. In contrast, the effect of recoil is noticeable as the surface temperatures are much higher and the heating rate is a few 100K in less than 5ms. The recoil pressure stretches the melt surface

downward, leading eventually to rupture. The plate oscillations have low amplitude in part because the spot is larger, and so the distance between the constrained outer plate edge and inner plate edge is shorter. Additionally, the melt reproduces the dripping dynamics as observed in Figure 5. Note that after the plate is ruptured, the remaining plate material starts to cool since the ruptured surface is less exposed to the laser beam.

For both laser spot sizes, the rupture leads to a diagonal melt that detaches from the center and swings towards the colder backside between 45*ms* and 55*ms*. The swinging arm remains attached to the plate since the plate is colder and hence the surface tension is higher. A similar melt swinging below the plate and landing on a random location away from the center is observed in the experiment (**Figure 1**). The larger spot size offers more material to the swinging motion and few flying debris. For the larger size, some liquid even touches the plate from below and locally melts it. This is indicated by the black contour lines, which correspond to zero shear modulus, i.e. to a liquid state.

6. DISCUSSION

It is important to have a grasp of the physics that was not include in the simulation and how these approximations could affect the quality of the analysis. First, the material evaporation effect on cooling the surface temperature is ignored. Evaporation is always present, but it is expected to be more important at very high laser intensities. Evaporative cooling would lower the surface temperature, which would increase the surface tension. Combined with evaporated material losses at very high laser intensities, the thinning of

the heated spot would be accelerated. The overall effect is a faster surface rupture. Hence, the current results can be viewed as an upper bound on time estimate for rupture.

A more complete evaporative model would have to include laser-screening effects. This can become very serious if the laser manages to ionize the vapor plume. In this case, the plasma can efficiently absorb the laser energy and prevent the surface rupture. It was shown (G. Tahmouch, 1997) that scaling down on laser intensity simply solves this problem. Given that the highest temperatures where still lower than boiling temperature for Aluminum, means that this regime was not crossed.

Other more complicated effects that are ignored pertain to the surface chemistry, which directly affects the laser absorptivity and can promote other thermally activated processes. This is a main unknown that would require further experimental measurements to feed into the material model input.

The choice for laser intensity depends much on the application. For example, in remote laser demining, time is not of essence. The low intensity laser would be enough to achieve the objective. The simulations show that the material at the laser spot coalesces into a large droplet with few small random satellites. This leaves a clear open window for the laser to penetrate the shell and cause further damage. Equivalently, the heated droplets or fragments would land inside and indirectly cause damage. The same applies for high intensity laser. The gain in time is not that great considering the extra cost for high power lasers.

On the other hand, when the mine is buried, high power lasers would be needed to penetrate the soil on top. In this case, the laser beam would be attenuated, due to the screening from the vapors (degasing of soil and transformation of water humidity to

vapor) released by the soil. One can approximate the beam as a low intensity laser by the time it hits the target. The latter would be heated enough for it to undergo deflagration.

7. CONCLUSION

In conclusion, the laser-material interaction is initially driven by the elastic-plastic response of the thin plate. The plate buckles up in the first few *ms* of the laser heating. At the onset of melting, thermal stress is relieved and the plate oscillates. This motion is coupled to the melt via the surface tension. The molten surface undergoes some oscillation cycles before other mechanisms cause plate rupture. The surface tension acts to thin a narrow band between the center of the plate and the edge of the laser spot region, hence initiating rupture. At very high laser power, surface tension decreases and vapor recoil pressure increases. The latter helps rupture the plate at the thinning band significantly sooner. The gravitational force is always present but tends to act at long time scales; hence, it is more evident at lower laser intensity. The simulations show symmetric rupture, due to the problem setup. However, the mechanisms of the plate rupture and droplet formation described here still hold in the case where the symmetry is broken due to surface anisotropies observed in the experiment.

8- ACKOWLEDGEMENTS

We would like to thank Al Nichols III for his help with the thermal package in ALE3D. This work was performed under the auspices of the U.S. Department of Energy by Lawrence Livermore National Laboratory under Contract DE-AC52-07NA27344. This

work was funded by the Laboratory Directed Research and Development Program at LLNL under project tracking code 12-ERD-050. The LLNL document review and release number is LLNL-JRNL-666426.

Bibliography

A. Klotzbach, M. Lutke, A. Wetzig and E. Beyer. "Advanced Remote cutting of non-metal webs and sheets." *Proceedings of ICALEO.* Orlando, 319-322, (2009).

A. Wagner, M. Lutke, A. Wetzig and L. M. Eng. "Laser Remote-Fusion Cutting With Solid State Lasers." *Journal of Laser Applications* 25, no. 5, 1-8, (2013).

A.M. Rubenchik, S. Wu "Temperature dependent 780-nm laser absorption by engineering grade aluminum, titanium and steel alloy surfaces." *Opt. Eng.* 53, no. 12 122506, (2014).

A.T. Dinsdale, P. N. Quested. "The viscosity of aluminum and its alloys-A review of data and models." *Journal of Materials Science* 39, 7221-7228, (2004).

Enrica Ricci, Donatella Giuranno, and Natalia Sobczak. "Further Development of Testing Procedures for High Temperature Surface Tension Measurement." *Journal of Materials Engineering and Performance* 22, 3381-3388, (2013).

G. F. Antonova, G. G. Gladush, F. K. Krasyukov, N. B. Rodionov. "The mechanism of remote cutting of metals by CO2 laser radiation." *High Temperature Apparatuses and Structures*, 477-482, (1999).

G. Tahmouch, P. Meyrueis, P. Grandjean. "Cutting by a high power laser at a long distance without an assis gas for dismantling." *Optics and Laser Technology*, 307-316, (1997).

Heller, Arnie. "Laser Burrows into the Earth to Destroy Land Mines." *Science and Technology*, October, 8-9, (2004).

—. "Transparent Ceramics Spark Laser Advances." *Science and Technology Review*, April, 10-17, (2006).

Khairallah, Saad A. and Anderson Andy. "Mesoscopic Simulation Model of Selective Laser Melting of Stainless Steel Powder." *Journal of Materials Processing Technology* 214, no. 11, 2627-2636, (2014).

M. F. Zaeh, J. Moesl, J. Musiol, F. Oefele. "Material Processing with Remote Technology Revolution or Evolution?" *Physics Procedia*, 1875-3892, (2010).

M. Lutke, A. Klotzbach, T. Himmer, A. Wetzig, E. Beyer. "Remote Cutting - One Technology Fits for Various Materials." *Lasers in Manufacturing .* Munich, 221-398, (2009).

M. Lutke, A. Mahrle, T. Himmer, L. Morgenthal and E. Beyer. "Remote Cutting - A Smart Solution Using the Advantages of High Brightness lasers." *ICA-LEO.* Miami: Laser Institute of America, (2005).

Macken, J. "Remote laser welding." *IBEC '96 Advanced Technologies and Processes.* Warren: Warren, Mich. : Automotive Technology Group, Inc., 11-15, (1996).

McCallen, R. "ALE3D: Arbitrary Lagrange Eulerian Three- and Two Dimensional Modeling and Simulation Capability." *LLNL-ABS-565212.* Livermore, CA: Lawrence Livemore National Laboratory, July 18, (2012).

R. P. Abbott, C. D. Boley, S. N. Fochs, L. A. Nattrass, J. M. Parker, A. B. Rubenshik, J. A. Smith, R. M. Yamamoto. *High-Power Solid-State Laser: Lethality Testing and Modeling.* Livermore: Lawrence Livermore National Laboratory, (2006).

R. S. Matti, T. Ilar and A. F. H. Kaplan. "Analysis of Laser Remote Fusion Cutting Based on a Mathematical Model." *Journal of Applied Physics* 114, 1-9, (2013).

Smurov, Gennady G. Gladush and Igor. "Physics of Laser Material Processing- Theory and Experiment." *Springer Serires in Materials Science.* Berlin, Heidelberg: Springer-Verlag, March, (2011).

Steen, W. M. *Laser Material Processing.* London: Springer, (2003).